AIChE

Detailed Analysis of Air Flow and Spray Loss in a Pharmaceutical Coating Process

Gregor Toschkoff and Daniele Suzzi
Research Center Pharmaceutical Engineering, Graz, Austria

Walter Tritthart, Franz Reiter, and Merten Schlingmann
G.L. Pharma GmbH, Lannach, Austria

Johannes G. Khinast
Research Center Pharmaceutical Engineering, Graz, Austria

Institute for Process and Particle Engineering, Graz University of Technology, Graz, Austria

DOI 10.1002/aic.12681
Published online June 16, 2011 in Wiley Online Library (wileyonlinelibrary.com).

In the pharmaceutical industry, more than half of all tablets receive a film coating. A commonly used technique is drum coating, where a film solution is applied to the moving tablets by a spray nozzle. Important process parameters include the amount and temperature of drying air, as well as spray nozzle position. Among other influences, the proper adjustment of these parameters has a great impact on spray loss, defined as the fraction of spray liquid that does not form a film on the tablets. Often, the lack of scientific data hinders a process setup based on engineering principles, resulting in operational conditions based on trial-and-error approaches. Here, we show how a coating system can be numerically modeled by means of computational fluid dynamics (CFD) techniques. Furthermore, we present how different parameters affect the efficiency of the process, leading to a deeper understanding of the coating device. © 2011 American Institute of Chemical Engineers *AIChE J,* 58: 399–411, 2012
Keywords: multi-phase flow, computational fluid dynamics, pharmaceuticals, tablet coating, spray loss

Introduction

For many pharmaceutical products, the application of a coating layer to tablets or granules is an important step in the production process. According to the IMS Midas Database for 2007,[1] for more than 50% of all tablet products, applying a coating is part of the production process. The purpose of coating application can be roughly divided into two categories: (1) functional and (2) non-functional. Functional coatings are used for taste or odor masking, to change the dissolution behavior or to add additional active ingredients. A non-functional coating is, for example, a colored outer layer whose sole purpose is the increase of visual attractiveness and recognition value.

In all of these cases, both intra-tablet and inter-tablet uniformity of the film is of great importance.[2] Intra-tablet uniformity is a measure of the variation of film thickness on a single tablet, whereas inter-tablet variation is the difference in film mass and quality between different tablets. If, for example, the purpose of the film is to protect the API from gastric juices, a single tablet with insufficient film thickness or quality can lead to the rejection of the whole batch.

In the course of the coating process, a tablet normally passes through a spray zone multiple times, where each time a partial coating layer is applied. For a single tablet, the time between two coating events, as well as the local film

Correspondence concerning this article should be addressed to J. G. Khinast at khinast@tugraz.at.

distribution in a single coating event, can differ considerably. If the variation between two events is large, a large number of partial coatings have to be applied to reduce statistical variance and to get a uniform coating layer. This way, the varying and poorly controlled conditions for a single event can be statistically compensated by the high number of tablet passes under the spray region. However, this results in a drastic increase in process time and, as a consequence, a decrease in efficiency. Therefore, it is highly desirable to understand and control the coating process as well as possible.

In this study, we focus on pan coaters, where tablet cores are placed in a rotating drum, and a film-building liquid is applied to the moving tablets by means of one or more spray nozzles. In every real, non-idealized tablet coating process, there is a certain percentage of liquid that does not end up forming a film on the surface of the tablets. This so-called spray loss is known as a critical issue for many surface treatment applications, for example, in the paint, coating, and metallurgical industry[3] and is encountered in the pharmaceutical industry as well, for example, in particle and tablet coating[4] or fluidized bed devices.[5] A corresponding quantitative indicator is the spray yield, that is, the ratio of the deposited spray material mass to the total mass introduced. For pan coating, the spray loss can be divided into two components:

- the liquid that ends up forming a film on the coating apparatus and
- the non-depositing droplets that are removed with the drying air.

The problem associated with the first component lies in the increased efforts necessary during the cleaning process. The second component consists of partially or totally dried spray droplets, which are contained in the exhaust air and in most cases have to be removed by means of a filtering system before the drying air can be allowed into the environment. Eventually, the filters have to be cleaned or disposed, introducing an additional time- and cost-consuming component to the process. Thus, minimization of spray loss represents an important factor for the enhancement of efficiency and profitability of the coating process

Another important topic in aqueous tablet coating is the water content of the air inside the coater. In many cases, the tablet cores are sensitive to water, and humidity should be kept as low as possible. The acceptable range of water content cannot be stated in general, and largely depends on the properties of the tablet cores and the film forming liquid. Although it is possible that problems arise from too dry tablet surfaces, normally the more significant concern is an over-wetting of tablets (as this may lead to hydrolysis of the API in the final formulation). However, the spray coating process as such demands the application of a water- (or solvent-) based liquid. As a result, it is desirable that the water (or solvent) is removed fast and efficiently by the drying air, in this way maximizing the spray rate that can be used without over-wetting the tablet bed. Thus, the drying capacity of the system should be maximized.

To a large extent, coating quality and especially spray losses depend on the quality of the spray produced by the nozzle. The most important parameters in this context are size and velocity distribution of the spray droplets. Also, as stated above, a significant amount of drying air has to be introduced, creating a pronounced air movement throughout the device. The behavior of the spray droplets after leaving the nozzle, and with it the amount of spray loss, depends to a large part on this air stream inside the coater.

Traditionally, the optimization of pharmaceutical processes is often based on empirical analysis. Although many input variables can be monitored in an experimental setup,[6] an analysis of the spray's behavior in the coating process by experimental measurements is hard to accomplish, especially for a production-scale coating apparatus. An alternative approach that sees increased use nowadays is the application of modern computational simulation tools. They allow overcoming some of the limitations of experimental measurements, thus offering the opportunity to get a deeper understanding of the process. So far, computational investigations of coating processes have mainly concentrated on two aspects: the statistics of the tablet movement[7,8] and the local film formation on the tablet surface.[9,10] To our knowledge, apart from a work on the influence of different parameters on the spray shapes in a lab coater,[11] no work has been published focusing on the description of the drying air stream inside the coater and its influence on the spray.

The aim of this work is a novel application of computational fluid dynamics (CFD) to study the air stream inside an industrial-scale pan coater and its impact on the spray behavior inside the coater. The effects of air flow, spray nozzle position, and orientation on spray loss and product quality were investigated. The following steps were performed:

- Determination of the size and velocity distributions of the spray droplets by means of PDA measurements;
- Implementation of the spray in the CFD simulations in accordance with the measurements;
- Modeling of the deposition on the tablet bed, the coating process, the evaporation of the spray and the wall film to estimate the effects of the drying gas flow;
- Post-processing of the simulation data to arrive at both qualitative and quantitative conclusions.

In the next section, the setup of the investigated pan coating system is described. First, the geometry of the pan coater is reported, followed by the definition of the operating conditions. Next, the experimental characterization of the spray is presented and the adopted numerical methods are then described, followed by the results of our numerical investigations. Finally, a detailed discussion of the results and a conclusion is presented.

Materials and Methods

In the following, the coating system used for the investigations is described. Process parameters are presented, the positions of the tablet bed and the spray nozzle are provided, and the spray characterization by the application of PDA measurements is described.

Characterization of the coating system

A drum coater with a non-perforated rotating drum (Nicomac Coating System classic 350, Nicomac srl, Italy) was investigated. Figure 1 shows a schematic drawing of the coating process. Along the rotational axis of the coating

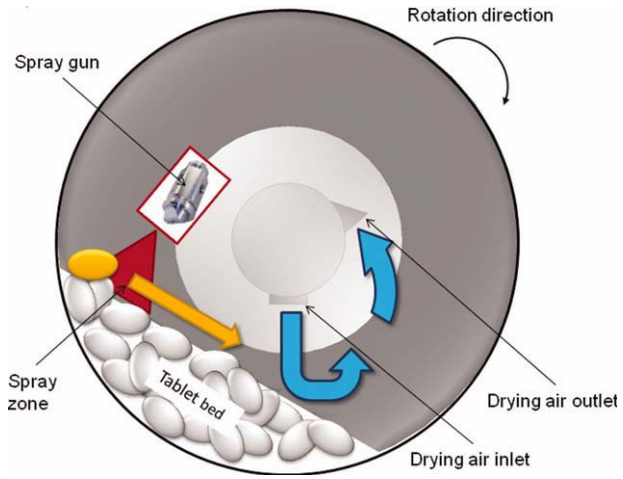

Figure 1. Schematic representation of a coating process in a drum coater.

A tablet emerging on the top enters the spray zone and the drying air zone before re-entering the bed. [Color figure can be viewed in the online issue, which is available at wileyonlinelibrary.com.]

drum, separate channels for incoming and outgoing drying air are located inside a metallic cylinder. At the upper left of the cylinder, the spray gun system is mounted. The drying air enters the drum at the bottom of the cylinder and the exhaust air is removed at the upper right location. The parameters characterizing the coating process are listed in Table 1. These values were used to define the boundary conditions of the simulation. The stated horizontal angle of the tablet bed was estimated visually, and was subject to change during the process as the growing coating layer alters the friction between tablets and coater.

In the process, the film solution is applied via two-component air-liquid nozzles (Schlick model 930 Form 7-1 S35 ABC, Schlick Atomizing Technologies, Germany). A peristaltic pump is used to transport the liquid through the hole located at the center of the nozzle tip. The spray atomization is assured by pressurized air (termed atomizing air) that flows through a circular opening surrounding the tip at a high velocity relative to the liquid velocity. Following the manufacturer recommendations, a second air stream (termed pattern air) from two additional outlets at the nozzle front is activated as well. This is done to alter the spray pattern from a circular to an elliptical cross-section with increased mass flow uniformity.

PDA measurement of spray properties

Measurements of the spray characteristics were performed using the phase-Doppler anemometry (PDA) technique.[12] It is capable of simultaneously measuring the particle diameter, velocity, and mass flux of spray droplets.[13] Because of the high spatial resolution and ease of use, spray characterization using PDA systems has found widespread application.[14,15] In early systems, the two best-known sources of error have been Gaussian beam effects and slit effects. Both can be greatly reduced by using a dual-mode PDA, where a standard PDA is combined with a planar PDA system.[16] Therefore, in this work a dual-mode PDA system (DANTEC DualPDA, Dantec Dynamics A/S, Denmark) was used for the characterization of the spray under realistic operating conditions. The measuring system consisted of a laser generating unit, a transmitter unit emitting the laser, a detector (58N81), and a processor connected to a personal computer (Flow and Particle Processor BSA 60). The two laser beams of 514.5 nm and 488 nm wavelengths were generated by an Argon-Ion laser and introduced into the transmission unit via fiber optic cables. The scattered light was measured and pre-processed by the Dual-PDA system. The raw data, including the diameters and velocities of every single measured droplet, was transferred to a personal computer. In a post-processing step, histograms were created, giving the frequency distribution of the measured quantities across all droplets of a single measurement.

For the PDA measurements, the same spray gun as in the Nicomac coating system was used. As the spraying liquid, a preparation of a methacrylic acid copolymer dispersion (Eudragit L30D-55, Evonik Röhm GmbH, Germany[17]) was used. Water was added to the commercial form, that is, an aqueous dispersion with 30% dry substance, until a percentage by weight of ~20% of dry substance was reached. The viscosity of the final dispersion at room temperature was 1.7 mPa s. For the nozzle operation, the atomizing air and pattern air pressure was 1.2 bar. The liquid flow rate was 60 g/min. The values were chosen according to nozzle manufacturer recommendations and practical experience from an industrial coating process.

Figure 2 shows the central part of the experimental setup. The laser beams enter from the left, and the bright area near $y = -40$ shows the measurement location, that is, the crossover region of the four laser beams inside the spray. The spray nozzle is located in the foreground on the right-hand side; in the background the receiver unit can be seen. The distance of the measurement point from the nozzle exit was 0.2 m, approximating the distance from nozzle to the tablet bed recommended by the manufacturer. Measurements were done for nine different positions from −80 mm to 80 mm with an interval of 20 mm along the horizontal spray axis, as shown in Figure 2. From the data sets for all positions, a mean value was calculated.

Numerical Model

For the numerical simulation of the dynamics of the air flow and the coating spray, the CFD (Computational Fluid Dynamics) code AVL FIRE[18] (AVL LIST GMBH, Austria) was used. The model of the coating process included three subsystems:

Table 1. Parameters Defining the Coating Process

Coater Parameter	Value
Drum diameter at the front/back	0.6 m
Drum diameter in the middle	1.5 m
Drum length	1.6 m
Tablet bed horizontal angle	~30°
Inlet air flow	1500 m^3/h
Inlet air temperature	60°C
Outlet pressure relative to atmosphere	−20 Pa
Tablet bed weight	300 kg
Tablet bed temperature	35°C
Rotation velocity	6 rpm

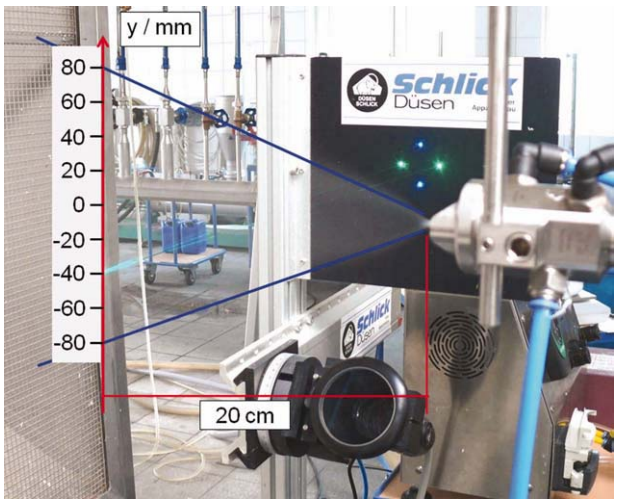

Figure 2. Picture of the experimental setup, showing the spray gun on the right and the receiver unit at the bottom.

The laser beams are entering from the left, the beam crossing area (measurement zone) can be seen at position −40. [Color figure can be viewed in the online issue, which is available at wileyonline library.com.]

- the air flow inside the coater
- the motion of spray droplets in the air stream
- the deposition of spray on surfaces as a wall film

Additionally, multi-phase evaporation of the coating liquid from the spray droplets, as well as from the wall film, was considered.

In our work, the common Reynolds-Averaged Navier-Stokes (RANS) approach was used to resolve the gas flow. This included the Reynolds-averaged forms of the conservation equations for mass, momentum, energy, as well as gas species. For closure of the equations, a standard $\kappa-\varepsilon$ model of the turbulent flow[19,20] was applied. The numerical solution of the problem was carried out in two steps. First, the air flow without spray was calculated until a converged state, that is, a dynamic equilibrium, was reached. Then, a transient calculation was started, using the converged steady-state as initialization. The spray was "introduced" into the air stream for a predefined time. To reduce calculation time, the spray droplets were simulated as parcels. A single parcel represents a certain number of identical droplets (the concept is explained in detail in the section on the spray module below). For each time step of the CFD calculation, the trajectory of the spray parcels was computed for a series of sub-steps. The necessary size of the sub-steps was determined automatically by the software based on the size of the CFD step and the parcel velocity. We were using a two-way coupling between continuous and solid phase. The application of numerical methods for the treatment of the droplet motion, the film formation and the evaporation is described in the next sections.

Mesh generation

On the basis of the geometry of the coater described above, a hybrid computational grid was generated, consisting of ~1.5 million cells of both tetragonal and hexagonal shape. As the coater pan was nearly symmetric with respect to a mirror plane normal to the rotational axis, only one half of the coater was considered, and symmetry boundary conditions were applied at the mirror plane. In Figure 3, a three-dimensional representation of the simulation regime (i.e., the back half of the coater) is shown. The cell size is automatically refined, that is, near critical regions, such as the tablet bed wall or the air inlet, the size of the cells is decreased and, therefore, resolution is increased. Position and angle of the wall are taken from observations of an industrial coating process (see Table 1). The observations also showed that the tablet bed in the used coating pan is relatively flat for moderate to high fill levels. For the simulation, the tablet bed could therefore be represented by a moving wall with reasonable accuracy. However, for a coating apparatus with pronounced baffles, or for low fill levels, this assumption would not work.

Although it is not feasible to resolve every single tablet at the tablet bed surface, a model for the treatment of the surface roughness has been applied, which takes the effects of roughness into account by an additional term in the wall function, directly modifying velocity at the wall. The surface roughness model needed the mean height of the roughness, that is, the typical difference between high and low areas on the surface. As an estimate, half the height of a tablet was chosen.

Spray module

In general, an aqueous coating solution consists of several components, including a suspended polymer in water, as well as additional additives in smaller quantities (e.g., talcum). Here, it was assumed that for the droplet movement and deposition, the exact composition has little influence, as long as macroscopic properties, such as density and viscosity, were modeled realistically. Therefore, for simplicity the

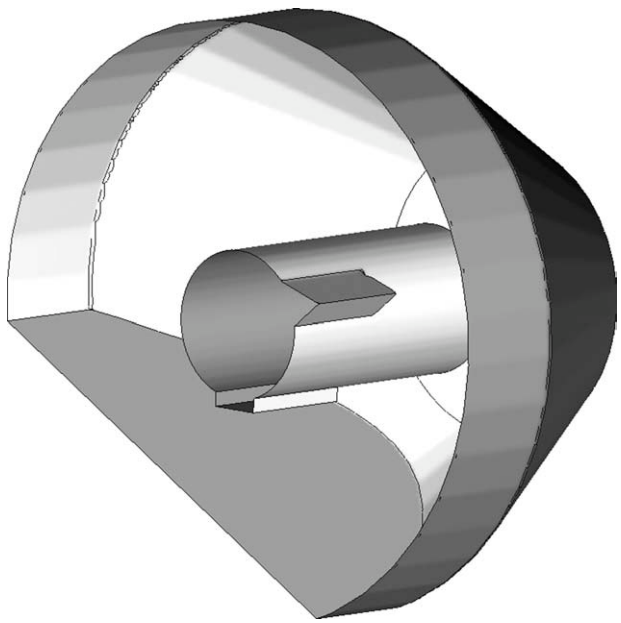

Figure 3. Three-dimensional graphic of the back half of the coating drum.

The cylinder along the rotation axis in the middle holds the air inlet and outlet. The tablet bed is approximated by a moving (straight) wall at the lower left.

spray was assumed to consist of only two substances, 80% water and 20% glycerol, the latter representing the film-forming polymer and additional components, similar to the approach suggested by Aliseda et al.[21] The physical properties of glycerol were taken from the manufacturer's specifications (The Dow Chemical Company, 2009).

The motion of the spray droplets was tracked using a Lagrange Discrete Droplet Method (DDM), based on the model of Dukowicz.[22] Because of a large number of droplets in the spray, it was not feasible to evaluate the encountered equations for every single droplet. Instead, we used the common statistical approach, where a group of identical droplets is represented by a single parcel. The amount of droplets in a parcel was calculated according to the given spray rate. In this way, the calculation time was greatly reduced without altering the statistical results. For each CFD time step, the Lagrange DDM equations were evaluated at a series of sub-steps for each parcel.

The movement of droplets is governed by Newton's equation:

$$m_d \frac{d\mathbf{u}_d}{dt} = \mathbf{F}_d + \mathbf{F}_G + \mathbf{F}_p, \tag{1}$$

with $\boldsymbol{u}_d$ being the droplet velocity. The drag force $\boldsymbol{F}_d$ is given as

$$F_d = \frac{1}{2}\rho_g A_d C_D |u_{rel}| \cdot u_{rel} \tag{2}$$

where A_d is the projected area of the droplet, u_{rel} is the relative droplet velocity, and C_D is the drag coefficient. The force $\boldsymbol{F}_G$ is a combination of gravity and buoyancy force, that is,

$$\boldsymbol{F}_G = V_d\left(\rho_d - \rho_g\right)g, \tag{3}$$

and $\boldsymbol{F}_p$ is the pressure force:

$$\boldsymbol{F}_p = V_d \nabla p. \tag{4}$$

Equation (1) was solved by direct time integration for each Lagrangian sub-step. The DDM incorporated a two-way coupling between the continuous and disperse phase, that is, the influence of the air flow on droplet motion as well as that of the droplets on the surrounding air was considered.

Mass and heat balance

The mass balance equation for a droplet is given as

$$\frac{dm_d}{dt} = -\dot{m}_E, \tag{5}$$

where m_d is the mass of the droplet. The only source term on the right hand side is the mass source for evaporation $\dot{m}_E$, other sources like droplet break-up by secondary atomization or droplet collision were neglected.

It was assumed that the temperature T_d inside a droplet is uniform. The droplet temperature decreases due to convective and latent heat loss, depending on the heat and mass transfer rate to the gas phase. The heat balance equation in the droplet is given by:

$$m_d \bar{c}_{p,d} \frac{dT_d}{dt} = -\Delta h(T_d)\dot{m}_E + \dot{Q}, \tag{6}$$

with $\bar{c}_{p,d}$ being the average of the specific heat capacity of all components of the droplets, Δh is the latent heat of evaporation, and $\dot{Q}$ the heat transfer rate between gas phase and droplets. Values with an over bar are evaluated at a reference temperature and reference gas composition, that is, at a location sufficiently far away from the droplet surface.

For the evaporation of spray droplets, a multi-component model based on the work of Abramzon and Sirignani was used,[23] with the extension of Brenn et al.,[24] allowing for separate evaporation of the liquid species. In this model, the mass transfer from the liquid to the gas phase was calculated separately for each component. The total evaporated mass was then the sum of the amount evaporated for each species $\dot{m}_E, j$. For the heat transfer, at the beginning mean values based on the liquid composition were calculated; the calculation then proceeded equivalent to a single-component model using the mean values. The evaporation model approach is based on the film theory, according to which the rate of evaporation $\dot{m}_E$ is calculated from the Sherwood and Nusselt numbers for mass and heat transfer, respectively. In the case of an evaporating droplet, corrected values of the Sherwood and Nusselt numbers, Sh^* and Nu^* are used. This is explained in detail below.

The mass transfer rate $\dot{m}_E$ in the mass and energy balances are:

$$\dot{m}_{E,j} = \pi \bar{\rho}_g \bar{D}_{g,j} d Sh_j^* \ln\left(1 + B_{M,j}\right), \text{with } \dot{m}_E = \sum \dot{m}_{E,j} \tag{7}$$

$$\dot{m}_E = \pi \frac{\bar{\lambda}_g}{\bar{c}_{p,d}} d Nu^* \quad \ln(1 + B_T). \tag{8}$$

The terms denoted with an overbar (i.e., thermal conductivity $\bar{\lambda}_g$, specific heat $\bar{c}_{p,d}$, gas density $\bar{\rho}_g$, and binary diffusion coefficient $\bar{D}_{g,j}$ of species j in the gas phase) were evaluated at the reference point.[25] d was the droplet diameter. In the Eq. (7) above, the Spalding mass transfer number $B_{M,j}$ was defined as:

$$B_{M,j} = \frac{w_{j,s} - w_{j,\infty}}{1 - w_{j,s}}. \tag{9}$$

Here, $w_{j,s}$ is the mass fraction of species j at the surface of the drop, to be calculated from the vapor pressure at the droplet temperature, and $w_{j,\infty}$ is the gas phase mass fraction in the bulk.

The Spalding heat transfer number B_T in Eq. 8 is given as

$$B_T = (1 + B_M)^{\Phi} - 1, \tag{10}$$

$$\Phi = \frac{\bar{c}_{p,d}}{\bar{c}_{p,g}} \frac{Sh}{NuLe}, \tag{11}$$

with $\bar{c}_{p,g}$ the gas phase specific heat capacity at the reference point and $\bar{c}_{p,d}$ the specific heat of the droplet liquid. The Lewis number Le is given as

$$Le = \frac{\rho c_p d}{\lambda}. \tag{12}$$

To calculate the temperature of the droplets from Eq. (6), the mass transfer rate $\dot{m}_E$ defined above, and the heat transfer rate $\dot{Q}$ between droplet and surrounding gas are needed. $\dot{Q}$ was defined as:

$$\dot{Q} = \dot{m}_E \left[\frac{\bar{c}_{p,d}(T_\infty - T_d)}{B_T} - \Delta h(T_d) \right]. \quad (13)$$

However, to calculate the heat transfer rate, the mass transfer rate has to be known, and vice versa. Therefore, for each time-step, a consistent solution had to be found by iteration.

To account for the relative motion of spray droplets and gas phase, the Nusselt number Nu and the Sherwood number Sh_j for component j were calculated from the Reynolds (Re), Prandtl (Pr), and Schmidt (Sc) numbers, according to empiric relations[26,27]:

$$Nu = 2 + 0.552 Re^{1/2} Pr^{1/3}, \quad (14)$$

$$Sh_j = 2 + 0.552 Re^{1/2} Sc_j^{1/3}. \quad (15)$$

The values of Nu and Sh_j above are correct for a non-evaporating droplet. As mentioned, the model is based on film theory, where heat and mass transfer is described by gas films of constant thickness. Therefore, the evaporation from the droplets was modeled with the aid of a virtual constant film. The thickness of the film was adjusted from classic film theory, this was taken into account by calculating the corrected Nusselt number Nu^* and Sherwood number Sh_j^* from the corresponding non-evaporating values as defined in Eqs. (14) and (15), and a correction function:

$$Nu^* = 2 + \frac{(Nu - 2)}{F_T}, \quad (16)$$

$$Sh_j^* = 2 + \frac{(Sh_j - 2)}{F_{M,j}}. \quad (17)$$

The temperature correction function F_T and mass correction functions $F_{M,j}$ have the same form, and are given as:

$$F_T = (1 + B_T)^{0.7} \frac{\ln(1 + B_T)}{B_T}, \quad (18)$$

$$F_M = (1 + B_M)^{0.7} \frac{\ln(1 + B_M)}{B_M}, \quad (19)$$

In Eq. (9), the mass fractions $w_{j,s}$ of the different liquid components j were needed. They were calculated from the mole fractions of each component at the droplet surface, given as

$$\chi_{j.s} = \chi_{j,d} \gamma_j \frac{p_{v,j}}{p} \quad (20)$$

Here, $\chi_{j.d}$ is the mole fraction inside the droplet, $p_{v,j}$ is the vapor pressure of species j and p is the total pressure. The activity coefficients γ_j for the water–glycerol mixture were calculated using a group contribution method, that is, the UNIFAC method.[28,29]

Wall film model

When modeling film formation on the walls of the coater (including the tablet bed), one can assume that the film thickness is much smaller than the wave length of variation in pressure along the walls. Therefore, one can assume that the film surface in each cell was parallel to the wall surface. Numerically, this meant that the simulation of the wall film was done in two dimensions, that is, in the plane of the wall surface. The advantage of a two-dimensional model was that no additional computational grid has to be generated for the film treatment. The thickness of the film was only entered as a scalar value for each existing cell, that is, the wall film thickness inside a single cell was constant. Thus, particular care was exercised to ensure that the computational grid of the coater close to the walls was sufficiently fine to ensure an excellent representation of the variation in film thickness. The time evolution of the wall film is governed by the film transport equation:

$$\frac{\partial \delta}{\partial t} + \frac{\partial u_1}{\partial x_1} + \frac{\partial u_2}{\partial x_2} = \frac{1}{\rho} s_m, \quad (21)$$

with δ being the thickness, and ρ the density of the wall film, s_m is the area-specific source term. To solve Eq. (21), the source term s_m and the mean velocity components u_1 and u_2 have to be calculated.

The mean velocity components were calculated from analytical velocity models, taking into account forces due to gravity, pressure gradients, and in-plane shear. Because of the low film thickness and thus small mass, inertial effects could be neglected, leading to a series of steady-state velocity profiles for each time step, greatly reducing the computational cost of solving the transport equation.

The source term consisted of film mass deposited by the spray as described in section below, and film mass lost by evaporation. The evaporation mass flux $\dot{m}_{E,j}$ from the film is described by Fick's law of unidirectional diffusion (Stefan diffusion):

$$\dot{m}_{E,j} = \left(\frac{\rho_g (D + D_t)}{1 - w_{S,j}} \right) \left(\frac{\partial w_j}{\partial y} \right)_S \quad (22)$$

Here, ρ_g is the density of the gas phase, D and D_t the molecular and turbulent diffusion coefficients, and w_j is the mass fraction of component j at the surface. The partial derivative $\partial w_j / \partial y$ is the concentration gradient of the mass fraction normal to the surface. The density ρ_g is calculated from the ideal gas law. For the diffusion coefficient D, empirical correlations were used, and $w_{S,j}$ could be calculated from the saturation pressure. This left the gradient of the mass fraction and the turbulent diffusion coefficient as unknown quantities. Here, they were modeled by using the boundary analogy of momentum and mass transfer, that is, the turbulent concentration profile and the turbulent diffusion process near to the liquid surface were modeled by using the analogy to the turbulent velocity profile.[25]

Spray Impingement

The model for spray impingement was based on the work of Mundo et al.[30] When a spray parcel hit a surface, it is either deposited on the wall or it splashes back, that is, the incident droplet breaks into smaller droplets. It has been

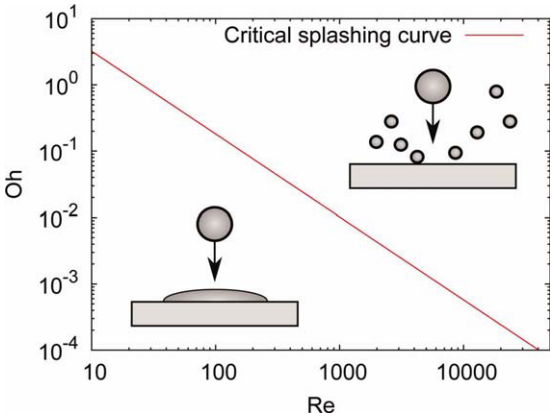

Figure 4. Ohnesorge number Oh as a function of Reynolds number Re.

The splashing region and the deposition region are separated by the critical splashing curve. [Color figure can be viewed in the online issue, which is available at wileyonlinelibrary.com.]

established that this process occurs depending on the dimensionless Reynolds number Re and Ohnesorge number Oh:

$$\mathrm{Re} = \frac{\rho_L v_d d}{\mu_L} \tag{23}$$

$$Oh = \frac{\mu_L}{\sqrt{\rho_L \sigma_L d}} \tag{24}$$

where ρ_L is the liquid density, v_d the droplet velocity, d the droplet diameter, and μ_L the liquid dynamic viscosity.

Mundo showed that when plotting the experimental data for Oh as a function of Re, the regimes of splashing and deposition are separated by a critical curve given as

$$Oh_{\mathrm{critical}} = 57.7 Re^{-1.25}. \tag{25}$$

The critical curve is shown in Figure 4. For the region over the critical curve, the droplets splash on impact. In this case, only a fraction of mass was transferred to the wall film. The rest did not deposit but formed newly generated droplet parcels. For the region under the critical curve, the complete liquid mass of the droplet parcel was transferred to the wall film.

Results and Discussion

In the first part of this section, the outcome of Phase-Doppler anemometry (PDA) measurements is presented. As mentioned above, the aim of these measurements was to provide the basis for realistic spray simulations. After that, the results concerning the air flow inside the coater and the spray simulations are described. Finally, indicators quantifying the process quality and the amount of spray loss are given for different nozzle configurations.

Spray characterization by PDA measurements

One of the most important quantities that influence the quality of the tablet film, and the coating process in general, is the size distribution of the spray droplets. For this reason, we first concentrated on the experimental characterization of the coating spray.

For good coating results, droplets should be roughly in the range of 10 μm to 60 μm. The measured distribution of the spray droplet diameter for standard operating parameters, that is, atomizing air and pattern air pressure of 1.2 bar and a liquid flow rate of 60 g/min, is shown in Figure 5. The shape of the distribution (an approximate Gaussian shape with a tail to higher droplet diameters) was typical for this kind of nozzle. It could be seen that nearly all droplets had a diameter smaller than 60 μm. A droplet diameter smaller than 10 μm was considered undesirable due to the large area-to-volume ratio: these particles could be already partially or completely dried before reaching a tablet surface, therefore forming a film of lesser quality, or not contributing to film formation at all. In Figure 5, ~38% of droplets, which is 4% of the total droplet mass, have a diameter smaller than 10 μm.

Numerical implementation of the spray

Although the output of the PDA measurements provided a distribution of the diameter and the velocity at a distance of 20 cm from the nozzle outlet, in the numerical simulation the spray was initialized by specifying the diameter and mass distribution of the spray parcels at the nozzle outlet. To ensure a correct correlation between measurement and simulation parameters the droplets were initialized according to the measured droplet diameter distribution. At a distance of 20 cm, diameter and velocity of the simulated spray were then compared to the experimental data.

It should be noted that coalescence was not taken into account, as for the two-component nozzle it can be expected that droplet interaction was negligible. A concern, however, was the correct velocity distribution at the tablet bed. In the real nozzle, atomizing and pattern air introduced a driving air flow. It was found that in the numerical simulation, these air flows can be omitted if a higher parcel starting velocity is chosen. After leaving the nozzle, the parcels were quickly decelerated by the drag force; in turn they accelerated the surrounding air and generated the required air stream. By using a velocity of $v = 180$ m/s it could be shown that the simulated spray is in good agreement with the PDA measurements. A comparison of the velocities at the tablet

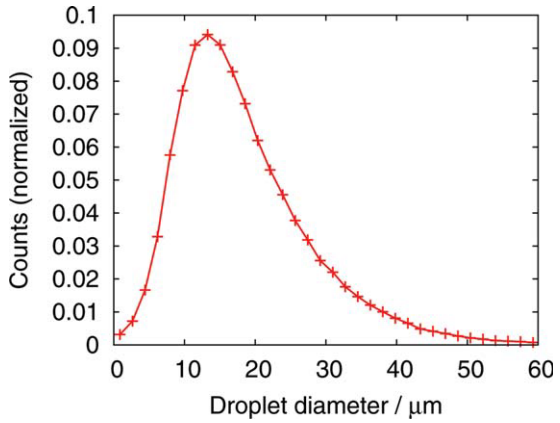

Figure 5. Number-weighted spray droplet size distribution in μm, as a mean of all positions in the PDA spray measurement at a distance of 20 cm.

[Color figure can be viewed in the online issue, which is available at wileyonlinelibrary.com.]

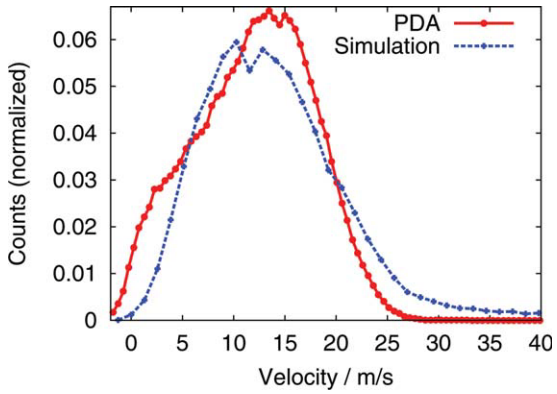

Figure 6. Number-weighted distribution of spray droplet velocities for experimental measurements (*o*) and CFD simulation (*x*).

By increasing droplet starting velocity, the lack of atomizing air flow was compensated such that the curves show good agreement. [Color figure can be viewed in the online issue, which is available at wileyonlinelibrary.com.]

bed for the simulation and the experiment is shown in Figure 6. It can be seen that the deviation between measurement and simulation was well inside acceptable boundaries, given the simplifying model assumptions. It is interesting to note that both the PDA measurement and the CFD simulation show a kink near the maximum of the curve, the origin of which was not conclusively known.

Simulation of the air flow inside the coater

To a large extent, spray droplet movement and tablet film formation are governed by the drying air flow. Thus, it is critical to understand the air flow in the coater. In the following section, the drying air flow is studied in more detail. To depict the nature of the air flow, different properties of the air are shown in two-dimensional plots using cut planes through the coater geometry. Figure 7 shows the location of the cut planes: (A) vertical through the nozzle position, (B) vertical behind the air inlet, and (C and D) are horizontal above and through the air inlet/outlet structure, respectively.

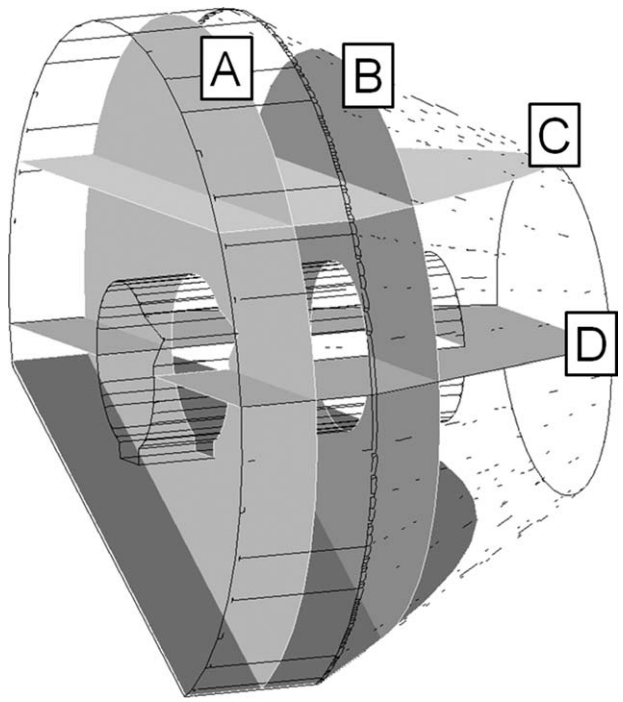

Figure 7. Location of the cut planes for the generation of two-dimensional plots inside the coater.

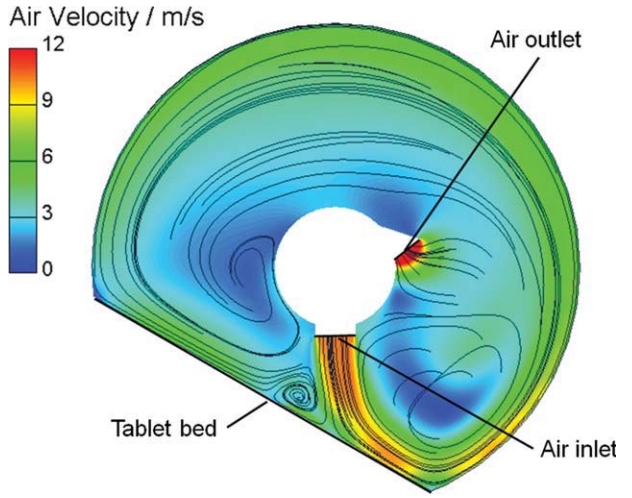

Figure 8. Air velocity for a cross-section through the location of the spray nozzle, perpendicular to the rotational axis.

Streamlines are drawn in black. [Color figure can be viewed in the online issue, which is available at wileyonlinelibrary.com.]

In Figure 8, the velocity of the drying air stream is shown for a cross-section through the coater, perpendicular to the rotational axis (plane A in Figure 7). As can be seen, the surface of the tablet bed was represented by a moving wall, that is, the missing circle section in the lower left part.

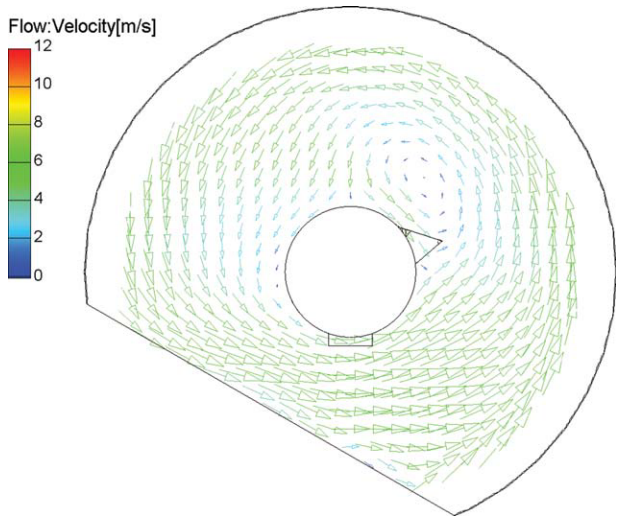

Figure 9. Vector plot of the air flow velocity inside cut plane B.

[Color figure can be viewed in the online issue, which is available at wileyonlinelibrary.com.]

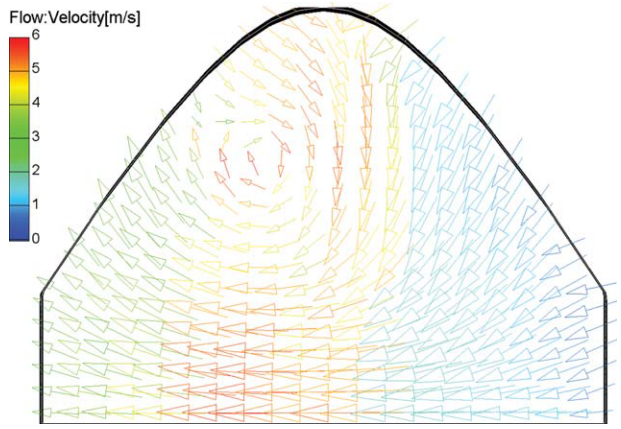

Figure 10. Vector plot of the air flow velocity inside cut plane C.

[Color figure can be viewed in the online issue, which is available at wileyonlinelibrary.com.]

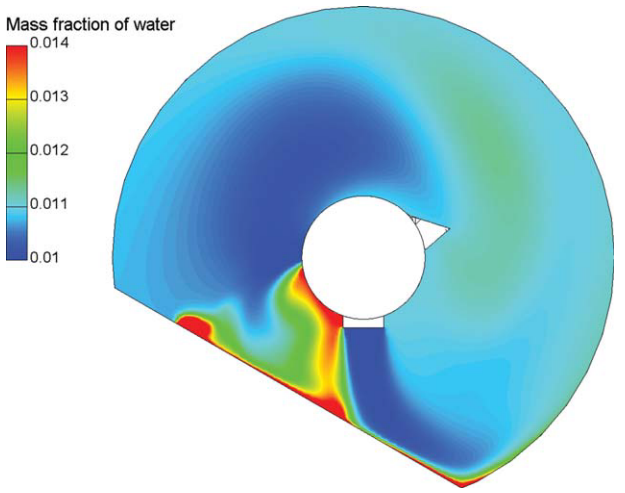

Figure 12. Mass fraction of water inside the coater.

[Color figure can be viewed in the online issue, which is available at wileyonlinelibrary.com.]

As expected, zones with increased air velocity existed near the inlet and outlet. Starting from the inlet, the drying air streamed downwards and hit the tablet bed. After drying the tablets coming from the spray zone located upstream, the inlet air had increased humidity and should leave via the outlet. However, as Figure 8 shows, instead the majority of air moved along the drum wall (against the rotational direction). Furthermore, a smaller portion of the inlet stream was not following the main flow, but formed an undesirable eddy between the spray zone and the area where the inlet air impacts the tablet bed.

The results suggested that a more effective removal of the humid air would be desirable. If feasible, one option could be the reduction of the inlet air flow rate, while increasing the inlet air temperature. Other possibilities include increasing the pressure drop at the outlet or installing a well-designed baffle system for the air outlet.

Figure 9 shows that the counter clockwise stream of the air that was seen above extended to the back section of the coater. As the air inlet and outlet did not cover the whole length of the coater, this section lied behind inlet and outlet. Without the direct air stream from the inlet to the tablet bed, the eddies near the tablet bed were not seen; however, eddy formation over the outlet region could be observed.

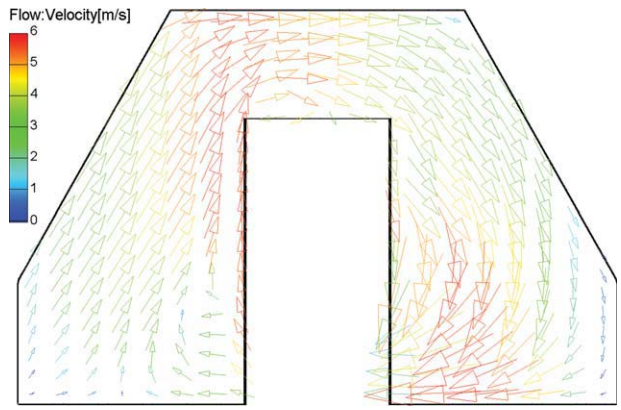

Figure 11. Vector plot of the air flow velocity inside cut plane D.

[Color figure can be viewed in the online issue, which is available at wileyonlinelibrary.com.]

The lateral air movement is depicted in Figures 10 and 11, the horizontal cuts through the coater. Note that the color scale has a maximum value of 6 m/s, compared to 12 m/s in the plots above. Overlaying the air flow against the coater rotation direction shown above, a rotational air flow in lateral direction took place. The air streamed from the middle of the coater to the end at the left side, and returned to the middle due to the lower pressure at the outlet.

Water content in the coater

For the incoming air, the humidity was set to be 0.01, resembling a typical value of environmental air. At the start of the simulation, the water mass fraction inside the coater was set to be 0.008 instead of 0.01, as it could be assumed that the dry and hygroscopic tablets will absorb some water from the environment. Without spray, in this setup the mean humidity would slowly rise from 0.008 to 0.01 with time, as the initial air was gradually replaced by fresh inlet air. If the additional water of the spray was included, the humidity would reach even higher values. Also, the humidity would be higher in areas directly affected by the spray, posing the risk of local over-wetting that could potentially damage the tablet cores. In Figure 12, the distribution of humidity, that is, the mass fraction of water in the gas, at 0.5 s after the start of spraying is shown. Regions of high water content could be seen in the areas where the spray hit the tablet bed and along the tablet bed, but also in the area between the tablet bed and the inner cylinder. The latter region originated from direct water evaporation from relatively small spray droplets carried over from the primary spray zone by the air flow. The picture was qualitatively the same for other times, with increasingly higher maximum water content. In Figure 13, the time evolution of the average mass fraction of water in the coater over the simulated period is shown. Although the water content increased steadily, it could be seen that the

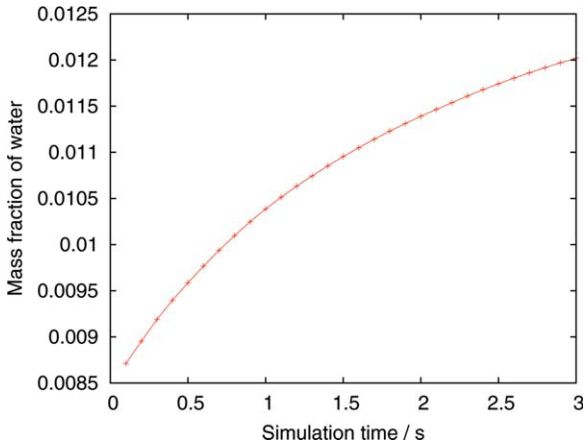

Figure 13. Average mass fraction of water in the coater as a function of time.

[Color figure can be viewed in the online issue, which is available at wileyonlinelibrary.com.]

rate of increase slows down with time, as in the long term a dynamic equilibrium with a constant average level of humidity had to be obtained. Although the average mass fraction of water was well inside typically acceptable limits, Figure 12 shows that the moisture near the tablet bed was ~1.6 times higher than the corresponding average value, meaning that local over-wetting could still occur.

The influence of nozzle placement on spray loss

In general, spray loss in drum coating occurs for two reasons. One part of the loss is made up of the spray droplets that are too dry to stick to a surface (spray drying phenomenon) or do not hit a surface at all. In both cases, the droplets eventually leave the device with the exhaust air. The other contribution to spray loss is spray liquid that forms a film on surfaces other than the tablets and has to be removed during post-process cleaning.

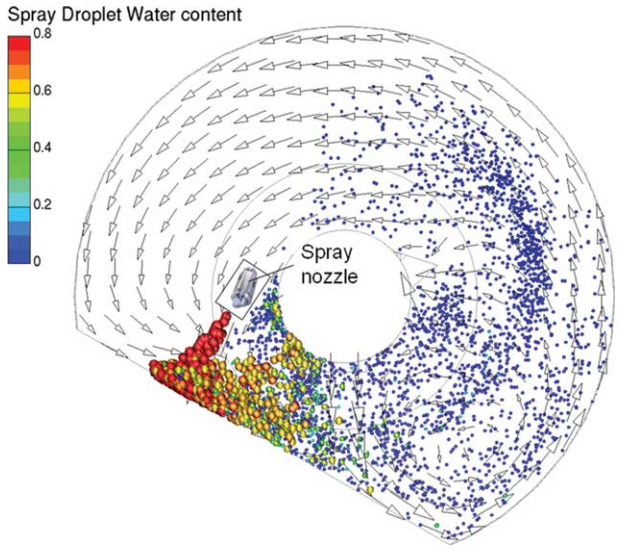

Figure 14. Spray after 0.5 s.

The color of the spray droplets show the amount of water, ranging from the starting concentration of 0.8 (red) to 0 (blue). The droplet size is proportional to the water content as well. Additionally, the air flow velocity is shown as a vector plot. [Color figure can be viewed in the online issue, which is available at wileyonlinelibrary.com.]

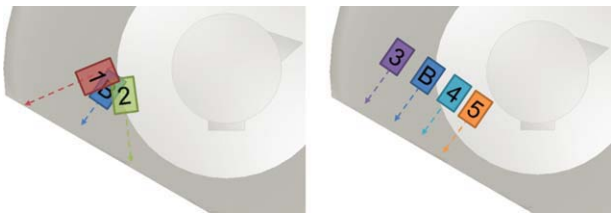

Figure 15. Variation of position and angle of the spray gun in the coating drum.

B denotes the standard position, 3–5 are variations translated parallel to the tablet bed. Cases 1 and 2 are a variation of the angle for basis position. [Color figure can be viewed in the online issue, which is available at wiley onlinelibrary.com.]

In Figure 14, the spray inside the coater after 0.5 s spraying is shown. The color and size of the droplets is proportional to the water content. The big droplets close to the spray nozzle still had a water content close to the initial spray water fraction of 0.8. The small droplets at the right-hand side were already partially or completely dried. It could be seen that a fraction of the spray moves towards the tablet bed, but was then dragged upwards and impacts the air inlet/outlet cylinder. The dry droplets that came close to the outlet leave with exhaust air. The rest of the droplets followed the flow of drying air and either left after several rotations with a varying residence time, or stuck to the rotating coater wall.

The figures concerning the air and spray flow discussed above provide a qualitative picture of the dynamics of the process. In the following, more quantitative measures are described. While in a numerical simulation arbitrary values for the operating parameters may be selected, strict regulations and cost concerns limit the parameters that can be changed for an already established industrial process. In this work, the parameter chosen for variation was the spray gun placement, which may be changed both in simulation and reality. Thus, an investigation of the influence of the nozzle position on the

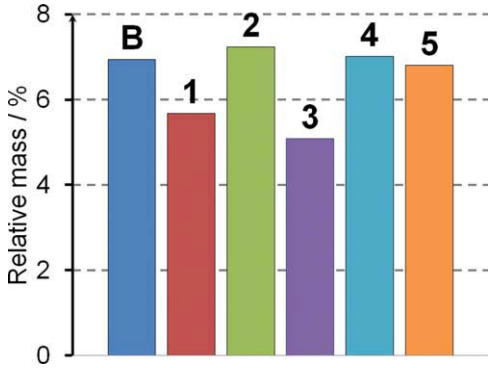

Figure 16. Total mass of the spray droplets leaving with the outlet air, relative to total introduced mass.

[Color figure can be viewed in the online issue, which is available at wileyonlinelibrary.com.]

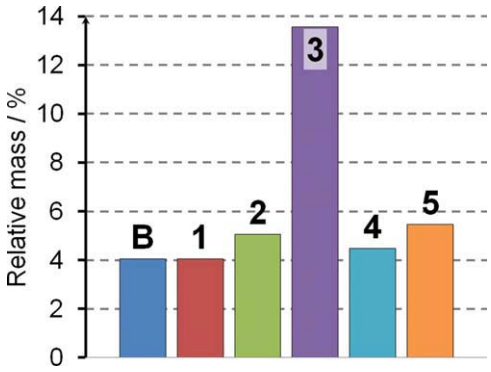

Figure 17. Total mass of spray droplets that hit a wall other than the tablet bed, relative to total introduced mass.

[Color figure can be viewed in the online issue, which is available at wileyonlinelibrary.com.]

coating process, especially on the amount of spray loss, was performed. These variations are shown in Figure 15. Starting from a base point (B), the spray nozzle was tilted away from (1) or towards (2) the air inlet. Additionally, a higher position (3) and two lower positions (4, 5) were selected.

Concerning the numerical work, the gas flow simulation was first started without spray until convergence was reached. Then, the spray was activated, and a time span of 3 s was simulated. The following key parameters were computed by integration over all simulation time steps to arrive at quantitative conclusions for the amount of spray loss:

- Spray mass leaving through outlet: the fraction of total liquid mass that had left the coater with the exhaust air
- Relative amount of film on the coater wall: The relative amount of liquid that formed a film on a surface other than the tablets.

The results are shown in Figures 16 and 17, respectively. When comparing the amount of spray loss for the different setups (Figure16), it can be seen that Case 1 and Case 3 performed better than the other cases, including the base case. ''Better'' in this case means that a larger percentage of the introduced spray stayed inside the coater instead of leaving with exhaust air. Taking the spray drying mentioned above into account, it can be concluded that the spray loss consisted largely of dried spray droplets.

From this information on spray loss only, it can be concluded that Cases 1 and 3 should be preferred, as in these cases the largest amount of spray stayed in the coater. However, this would not take into account where the coating liquid is to be found in the coater. To get more information on the liquid distribution, we calculated the relative amount of film formation on coater surfaces other than the tablet bed (Figure 17). In Case 3, a significant increase of unwanted material deposition was detected, showing that for this case, the low amount of spray droplets in the exhaust air comes with the price of increased deposition on coater surfaces. To examine this phenomenon in more detail, the distribution of the wall film after 3 s of simulation time for Case 3 was visualized, as shown in Figure 18. Apart from a coating of the tablet bed as expected, the rotating coater wall near the top of the tablet bed was showing film formation as well. In addition, a wall film was building up on the air inlet/outlet cylinder in the middle of the coater, on the side opposite of the outlet. Closer investigations showed that this phenomenon happened for all other nozzle positions, although to lesser extents. Film formation in the same locations has also been observed in industrial coating processes using the described coating equipment, underlining the predictive capability of the simulation model.

In summary, a reduction of spray losses compared to the standard operational conditions (B) was seen in Case 1 and Case 3. However, in Case 3 the reduction occurred because a large portion of the spray ended up forming a highly undesirable film on the rotating coater wall. Therefore, making a nozzle arrangement according to Case 1 was the optimum choice, where the spray loss was reduced without negative side effects by slightly tilting the spray nozzle away from the inlet.

Conclusions

In this study, we have presented the modeling of a pan coating process using CFD. A hybrid mesh was generated mimicking the geometry of a full-scale industrial coater. The critical process parameters (e.g., inlet air temperature, flow rate, and drum rotation speed) were selected according to standard operating conditions. A central part of each pan coater is the spray nozzle. To simulate the spray as realistically as possible, Phase-Doppler anemometry measurements were performed, using Eudragit L30D-55 filming solution to generate the basis for the ''numerical'' spray.

The results indicate that a detailed understanding of air flow inside a coater is necessary to optimize the dynamics of a coating process. As an important quantitative measure for the quality of the coating procedure, the spray loss was calculated. As variation parameters, different nozzle positions and directions were chosen. The rationale behind this choice

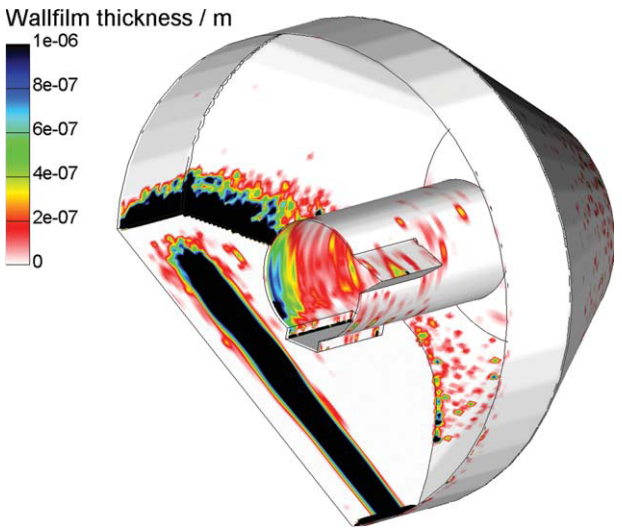

Figure 18. Wall film thickness on the coater wall, from no film (white) to a thickness above one micrometer (black).

It can be seen that apart from the tablet bed, film liquid is also deposited on the rotating wall near the tablet bed top and the middle cylinder. [Color figure can be viewed in the online issue, which is available at wileyonlinelibrary.com.]

was the fact that these parameters could be easily changed, even in an already validated process. Our results showed that the usual recommendation of placing the spray nozzle at a distance of one third of the total tablet bed length from the top of the tablet bed gave the best results. However, instead of orienting the spray strictly perpendicular to the tablet bed as is common practice, tilting the nozzle away from the inlet air showed a reduction in spray loss.

The model of the coater process described in this work was aimed to capture the fundamental phenomena leading to spray loss in an industrial coating process. Nevertheless, many aspects need to be further investigated. As a next step, the model will be expanded, for example, by increasing the number of spray nozzles or accounting for the elliptical shape of the spray. A more detailed description of the turbulent air flow through the tablet bed is desirable as well. In future, we also intend to apply more sophisticated approaches, such as the LES-LPT model that we developed recently.[31] The influence of a range of additional parameters, such as temperature, air flow boundary conditions, or nozzle type, will be investigated in the future.

In addition, the validation of the numerical results represents an important step in our future work. Thermal imaging of the coater's internal surfaces, or the quantification of the spray mass trapped inside the filters are some examples of our current activities. Furthermore, the coating efficiency on the tablet bed is to be quantified by means of Near-Infrared (NIR) spectroscopy online methods.

Notation

Latin symbols

A = area, m^2
$B_{M,j}$, B_T = spalding mass and heat transfer number, –
c_p = specific heat capacity at constant pressure, J/kg/K
C = drag coefficient, –
d = particle diameter, m
D = diffusion coefficient, m
F = force, N
$F_{M,j}$, F_T = mass and temperature correction functions, –
g = gravitational acceleration, m/s^2
h = specific enthalpy, J/kg
m = mass, kg
p = pressure, Pa
$\dot{Q}$ = heat transfer rate, W
R = pan radius, m
s_m = area-specific mass source, $kg/m^2/s$
t = time, s
T = temperature, K
u, v = velocity, m/s
V = volume, m^3
w = mass fraction, kg/kg
x = mole fraction, mol/mol
x_1, x_2 = Cartesian coordinates, m
y = space component normal to the wall, m
$y+$ = non-dimensional wall distance, –

Dimensionless numbers

Le = Lewis number ($=Sc/Pr$)
Nu = Nusselt number ($=\alpha L/k$)
Oh = Ohnesorge number ($=\mu/(\rho\sigma L)^{0.5}$)
Pr = Prandtl number ($=c_p\mu/k$)
Re = Reynolds number ($=uL/v$)
Sc = Schmidt number ($=v/\beta$)
Sh = Sherwood number ($=k_m L/b$)

Greek letters

γ = activity coefficient, –
Δ = variation, –
δ = wall film thickness, m
ε = turbulent dissipation, m^2/s^3
Φ = exponent for heat transfer calculation, –
λ = heat conductivity, $W/m^2/K$
μ = dynamic viscosity, Pa s
v = kinematic viscosity, m^2/s
ρ = density, kg/m^3
σ = surface tension, N/m
ω = pan rotational speed, rad/s

Subscripts and superscripts

$\dot{x}$ = rate of change or flux of variable x
∞ = bulk
– (overbar) = at the reference point
d = droplet
D = drag
E = evaporation
g = gas
G = gravity and buoyancy
i, j = index
I = interfacial
P = pressure
Rel = relative
S = surface value
v = vapor

Literature Cited

1. IMS Health C, USA. IMS Midas Database. 2007.
2. Tobiska S, Kleinebudde P. Coating uniformity and coating efficiency in a Bohle Lab-Coater using oval tablets. *Eur J Pharm Biopharm.* 2003;56:3–9.
3. Davis JR, editor. *Handbook of Thermal Spray Technology*. ASM International, 2004:126.
4. Rähse W. Produktdesign disperser stoffe: industrielles partikelcoating. *Chem Ingenieur Tech.* 2009;81:225–240.
5. Schreiber R, Vogt C, Werther J, Brunner G. Fluidized bed coating at supercritical fluid conditions. *J Supercrit Fluids.* 2002;24:137–151.
6. Ruotsalainen M, Heinämäki J, Rantanen J, Yliruusi J. Development of an automation system for a tablet coater. *AAPS PharmSciTech.* 2002;3: article 14.
7. Freireich B, Wassgren C. Intra-particle coating variability: analysis and Monte-Carlo simulations. *Chem Eng Sci.* 2010;65:1117–1124.
8. Mueller R, Kleinebudde P. Prediction of tablet velocity in pan coaters for scale-up. *Powder Technol.* 2007;173:51–58.
9. Kalbag A, Wassgren C. Inter-tablet coating variability: tablet residence time variability. *Chem Eng Sci.* 2009;64:2705–2717.
10. Suzzi D, Radl S, Khinast JG. Local analysis of the tablet coating process: impact of operation conditions on film quality. *Chem Eng Sci.* 2010;65:5699–5715.
11. Muliadi A, Sojka P. Implementation of Quality-by-Design Principles: Modeling of Spray Tablet Coating Using a CFD Approach. Paper presented at AIChE Annual Meeting 2009; Nashville.
12. Hirleman ED. History of development of the phase-doppler particle-sizing velocimeter. *Part Part Syst Char.* 1996;13:59–67.
13. Zaidi SH, Altunbas A, Azzopardi BJ. A comparative study of phase doppler and laser diffraction techniques to investigate drop sizes in annular two-phase flow. *Chem Eng J.* 1998;71:135–143.
14. Kim J, Kim J. A characterization of the spray evolution by dual-mode phase doppler anemometry in an injector of liquid-propellant thruster. *J Mech Sci Technol.* 2009;23:1637–1649.
15. Payri R, Tormos B, Salvador FJ, Araneo L. Spray droplet velocity characterization for convergent nozzles with three different diameters. *Fuel.* 2008;87:3176–3182.
16. Tropea C, Xu T-H, Onofri F, Géhan G, Haugen P, Stieglmeier M. Dual-mode phase-doppler anemometer. *Part Part Syst Char.* 1996; 13:165–170.

17. EVONIK Röhm GmbH. Specifications and test methods for EUDRAGIT® L 30 D-552007.
18. AVL LIST GmbH. FIRE v 2008 User Manual. 2008. Available at: www.avl.com/fire. Accessed on April 10, 2010.
19. Patel V, Rodi W, Scheuerer G. Turbulence models for near-wall and low reynolds-number flows—a review. *AIAA J*. 1985;23:1308–1319.
20. Wilcox D. *Turbulence modeling for CFD*, 2nd ed. La Canada CA: DCW Industries, 1998.
21. Aliseda A, Hopfinger EJ, Lasheras JC, Kremer DM, Berchielli A, Connolly EK. Atomization of viscous and non-newtonian liquids by a coaxial, high-speed gas jet. Experiments and droplet size modeling. *Int J Multiphase Flow*. 2008;34:161–175.
22. Dukowicz JK. A particle-fluid numerical-model for liquid sprays. *J Comput Phys*. 1980;35:229–253.
23. Abramzon B, Sirignano WA. Droplet vaporization model for spray combustion calculations. *Int J Heat Mass Transfer*. 1989;32:1605–1618.
24. Brenn G, Deviprasath LJ, Durst F, Fink C. Evaporation of acoustically levitated multi-component liquid droplets. *Int J Heat Mass Transfer*. 2007;50:5073–5086.
25. Piccioli R. *Injection and Combustion of Water/Diesel Fuel Emulsions. Analysis and CFD Modelling Based on FIRE 8.5*. Università di Bologna; 2006.
26. Ranz WE, Marshall WR. Evaporation from drops. *Chem Eng Progr*. 1952;48:173–180.
27. Ranz WE, Marshall WR. Evaporation from drops. *Chem Eng Progr*. 1952;48:141–146.
28. Attarakih M, Abu Fara D, Sayed S. Dynamic modeling of a packed-bed glycerol-water distillation column. *Ind Eng Chem Res*. 2001;40:4857–4865.
29. Peres AM, Macedo EA. A modified UNIFAC model for the calculation of thermodynamic properties of aqueous and non-aqueous solutions containing sugars. *Fluid Phase Equilibria*. 1997;139:47–74.
30. Mundo C, Sommerfeld M, Tropea C. Droplet-wall collisions—experimental studies of the deformation and breakup process. *Int J Multiphase Flow*. 1995;21:151–173.
31. Sungkorn R, Derksen JJ, Khinast JG. Modeling of turbulent gas-liquid bubbly flows using Stochastic Lagrangian model and Lattice-Boltzmann scheme. *Chem Eng Sci*. 2011;66:2745–2757.

Manuscript received Oct. 5, 2010, and revision received Apr. 11, 2011.